Journal of Stress Analysis
Vol. 9, No. 1, 2025, 95-108
Bu-Ali Sina University

ORIGINAL RESEARCH PAPER

Flexural Behavior of Fully Integrated 3D-Printed Sandwich Panels Versus Thermoplastic Cores with Composite Facesheets

Majid Moradi, Hassan Shokrollahi*
Department of Mechanical Engineering, Faculty of Engineering, Kharazmi University, Tehran, Iran.

Article info

Article history:
Received 10 April 2025
Received in revised form
22 June 2025
Accepted 25 June 2025

Keywords:
Sandwich panel
Three-point bending
Thermoplastic composite
Auxetic materials
3D printing

Abstract

In this study, the bending behavior of sandwich structures was investigated in both integrated and separate configurations. The structures featured honeycomb and re-entrant cores made from thermoplastic materials, Polylactic Acid (PLA) and Acrylonitrile Butadiene Styrene (ABS), fabricated using a 3D printer. Additionally, samples with composite facesheets, produced from glass fibers combined with chopped PLA or ABS filaments, were fabricated using a hot press machine. The composite facesheets, comprising two layers of glass fibers, were incorporated to enhance strength and resistance to environmental factors. The use of recyclable and remanufacturable structures contributes to environmental protection, pollution reduction, and lower production costs. The core dimensions were 15×50×160mm, with a facesheet thickness of 1.5mm. The weight of the sandwich structures ranged from approximately 42 to 70 grams, depending on the core geometry and facesheets used. In total, 24 samples underwent a three-point bending test, and 4 samples were subjected to a tensile test to determine the mechanical properties of the sandwich panels. The elastic modulus for PLA, ABS, composite PLA, and composite ABS samples was 2.83, 2.40, 24.71, and 23.82GPa, respectively. The bending test results indicated that samples with re-entrant cores withstood higher loads compared to those with honeycomb cores. The maximum load-bearing capacity and energy absorption of the composite-faced samples were superior to both the integrated and separate samples. Furthermore, the composite, separate, and integrated samples exhibited greater deflection, respectively, and failed later.

1. Introduction

The pursuit of optimal material utilization and high-performance structural designs has long been a central objective in engineering mechanics. Among the most widely used structural configurations across industries such as aerospace, automotive, marine, and construction are sandwich panels [1, 2]. These structures are favored for their exceptional properties, including high strength-to-weight and stiffness-to-weight ratios, excellent energy absorption, outstanding impact resistance, and superior thermal and acoustic insulation capabilities [3, 4]. Consequently, they are frequently employed in demanding applications where lightweight and durable materials are paramount.

A conventional sandwich panel consists of two thin, stiff facesheets bonded to a relatively thick, lightweight core. The facesheets primarily carry bending stresses,

*Corresponding author: H. Shokrollahi (Associate Professor)
E-mail address: hshokrollahi@khu.ac.ir
10.22084/jrstan.2025.31698.1271
ISSN: 2588-2597

while the core resists shear forces [5]. Numerous core designs are utilized, including foams, honeycombs, corrugated structures, and, more recently, advanced architectures such as auxetic geometries [6, 7]. Honeycomb cores, inspired by natural patterns, are prevalent due to their lightweight nature and enhanced mechanical properties compared to solid structures [8]. Auxetic materials, which exhibit a negative Poisson's ratio, have garnered significant interest in recent years. When stretched, these materials expand laterally, and when compressed, they contract laterally. This unique deformation mechanism can lead to improved shear resistance, indentation performance, and energy absorption [9, 10].

Facesheets can be metallic, polymeric, or composite. While metallic facesheets are simple and widely used [11], the trend in high-performance industries is shifting towards composite facesheets [12]. Composites, which can be polymer-, metal-, or ceramic-based, offer the distinct advantage of tailorability. By aligning fiber reinforcements with the direction of loading, they provide superior mechanical properties, thereby achieving significant material efficiency [13, 14].

Additive manufacturing (3D printing) presents a revolutionary approach for fabricating complex structures, including sandwich panels with intricate core topologies. Fused Filament Fabrication (FFF) using thermoplastics such as Polylactic Acid (PLA) and Acrylonitrile Butadiene Styrene (ABS) allows for the creation of integrated or separate core-facesheet configurations with high geometric freedom [15, 16]. PLA, a biodegradable thermoplastic derived from renewable resources, is particularly attractive for environmentally conscious applications [17]. ABS, another common thermoplastic, is recognized for its favorable mechanical properties, thermal stability, and impact resistance [18].

Driven by growing environmental concerns and the need to protect natural resources, there is an increasing emphasis on developing sustainable, recyclable, and remanufacturable structures [19-21]. This research aligns with that goal by focusing on the flexural behavior of sandwich panels fabricated using environmentally compatible materials and processes. The key novelty of this work lies in the direct comparison of three distinct manufacturing routes. This study investigates panels with porous cores (honeycomb and re-entrant) and facesheets made from thermoplastics (PLA and ABS) in both integrated (monolithic 3D printed) and separate (adhesively bonded) configurations. Furthermore, it introduces and tests a novel configuration: panels with 3D-printed thermoplastic cores and hot-pressed composite facesheets made from glass fibers and chopped recycled thermoplastic filaments (chopped PLA and ABS). This systematic approach allows for a clear evaluation of the synergy between manufacturing method, facesheet material, and core geometry, which is underrepresented in the existing literature.

The primary objective is to comprehensively compare the flexural performance, energy absorption capacity, and failure modes of these different sandwich panel architectures. By evaluating the synergy between core geometry (conventional honeycomb vs. auxetic re-entrant), facesheet material (neat thermoplastic vs. glass fiber composite), and manufacturing method (3D printing vs. hot pressing), this work aims to contribute to the development of high-performance, sustainable sandwich structures for advanced engineering applications. The three-point bending test was selected as it is a standard method (ASTM C393) for evaluating the overall structural performance of sandwich panels under out-of-plane loads, which simulates critical real-world conditions in applications such as vehicle body panels and building cladding.

2. Sample Fabrication and Testing Methods

Sandwich panels were fabricated in both integrated (monolithic) and separate (adhesively bonded) configurations using a 3D printer with ABS and PLA thermoplastics. Finally, samples with porous thermoplastic cores (honeycomb and re-entrant) and composite facesheets were produced. The composite facesheets were manufactured using a hot press machine, which is a highly effective method for this purpose. The use of composite facesheets helps increase strength and resistance to environmental factors.

2.1. Materials and Fabrication Process

The cores were made from PLA with two types of porous structures, honeycomb and re-entrant, fabricated using 3D printing technology. For the composite facesheets, glass fibers and resin from the same types of chopped PLA and ABS filaments were used. A hot press was used to fabricate the composite. Details of each fabrication step are provided below. The re-entrant and honeycomb cores with dimensions of 160×50×15mm were designed using SolidWorks software, as shown in Figure 1, and then fabricated using a 3D printer from ABS and PLA materials.

Fused filament fabrication (FFF) technology was used to fabricate the auxetic cores. eSUN brand filament was used; grey PLA filament and white ABS filament. The 3D printer was a SAMIN 3D model. The nozzle temperature for printing PLA was 215°C and the heated bed temperature was 60°C. The nozzle temperature for printing ABS was 250°C and the heated bed temperature was 90°C. The layer height was 0.2mm and the nozzle diameter was 0.4mm.

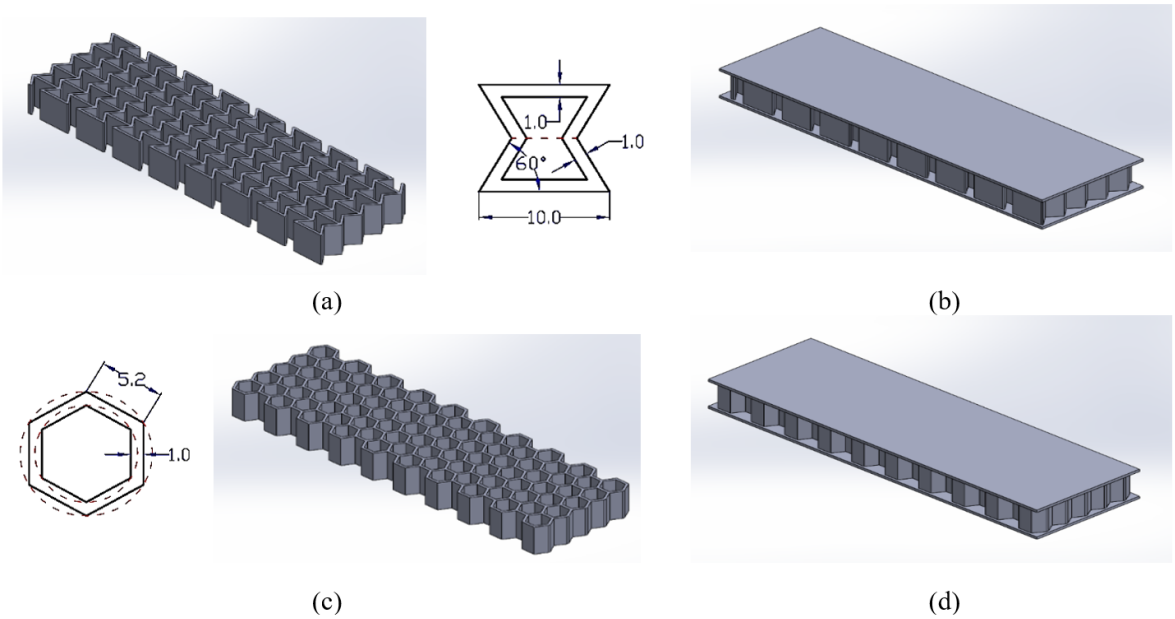

Fig. 1. Models designed in SolidWorks software.

A total of 24 samples were prepared for flexural testing: 8 samples with integrated cores and facesheets, 8 samples with separate core and facesheet, and 8 samples with separate cores and composite facesheets reinforced with glass fibers. Some printed samples are shown in Fig. 2.

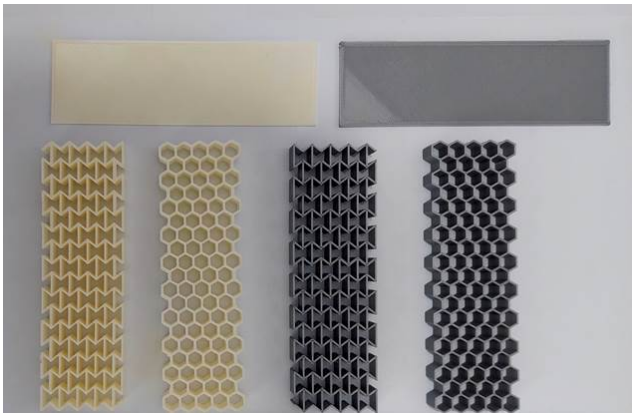

Fig. 2. The fabricated sandwich panel via 3D printer.

The process for manufacturing the composite facesheets using the hot press is described below.

The resin used in this research to fabricate the sandwich panel facesheets consisted of chopped PLA and ABS filaments. The filaments were shredded using a shredder for use in the hot press, as shown in Fig. 3.

In this research, a woven E-Glass fabric with a density of 400 g/m was used. E-Glass is one of the most widely used types of glass fiber in the composite industry. Sharp tools were used to cut the glass fiber fabric to minimize fraying and maintain fiber alignment, which is critical for structural strength. The glass fibers were cut to dimensions of 200×200mm, with each piece weighing approximately 16.2 grams.

The composite facesheets produced in this study had a thickness of 1.5mm, for which a mold with dimensions of 200×200×1.5mm was used.

Fig. 3. Layup of composite facesheets.

Initially, an attempt was made to use three layers of glass fiber. However, due to the small thickness of the mold and the slippery nature of the shredded filament pieces, fiber slippage and incomplete resin penetration in some areas of the glass fiber were observed. Ultimately, two layers of glass fiber fabric, cut to dimensions of 200×200mm, were used. The weight of each layer of glass fiber was approximately 16.2 grams, totaling 32.4 grams. The density of the glass fiber is 2.5g/cm^3. The volume of the glass fiber was calculated to be 12.96cm^3. Given the total mold volume of 60cm^3, the corresponding fiber volume fraction was approximately 21.6%. The schematic of the layup of the fibers and shredded filaments is shown in Fig. 4.

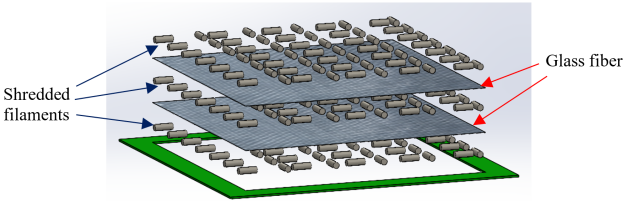

Fig. 4. Schematic of the composite facesheet layup.

After shredding the filaments and cutting the glass fiber, the composite fabrication stage began. In this research, a 15-ton hot press machine was used, and the press temperature was set according to the melting points of the polymers. Since the melting point of PLA is around 190°C and that of ABS is around 320°C, to ensure better resin flow and penetration into all parts of the fabric, the machine temperature was set to 210°C for PLA and 330°C for ABS. To prevent inter-layer slippage during the pressing process, two thick, heavy metal plates were used. Heat-resistant paper was placedbeneath and on top of the main mold to separate it from the metal plates.

After placing the sample in the mold and under the machine, it took about 15 minutes for the mold to reach the desired temperature. During this time, only the upper and lower plates of the machine were brought closer together to heat the mold faster. Initially, no pressure was applied. After the mold heated up and the resin melted, which took about 20 minutes, pressure application to the mold began. Pressure was applied in three stages: 40 bar, 80 bar, and 110 bar, with 2-3 minute intervals. After the initial 40 bar pressure was applied, excess resin was extruded from the sides of the mold, as depicted in Fig. 5.

After sufficient time under 110 bar pressure at the set temperature for the PLA and ABS matrix composites, the samples were removed from the hot press. To cool gradually and prevent warping, the samples were placed under a cold press at about 60 bar pressure for 10 minutes.

A diamond blade with a thickness of about 3mm was used to cut the composite samples to the desired dimensions.

In this research, a commercial cyanoacrylate adhesive (Type 502) was used to bond the cores and facesheets. Prior to bonding, all contacting surfaces were cleaned with isopropyl alcohol to ensure optimal adhesion. The adhesive was applied uniformly across the entire surface of the core using a dispensing nozzle. A constant pressure of approximately 5kPa was applied to the assembly for 2 minutes to ensure a thin and consistent bond line. The bonded samples were then left to cure at room temperature for 24 hours before testing. Bonding the facesheets to the core was a critical step in the sandwich panel fabrication process. Cyanoacrylate adhesive was selected for its rapid curing, high tensile shear strength, and ability to form a rigid bond.

(a)

(b)

Fig. 5. a) Hot press machine, b) Excess resin extruding from the mold after pressure application.

A rigid adhesive was chosen to minimize compliance in the bond line, thereby ensuring efficient stress transfer between the facesheets and the core during bending. The potential influence of the adhesive layer is inherently captured in the performance comparison between the 'Separate' (bonded) and 'Integrated' (monolithic) configurations, where any detrimental effect would manifest as a reduction in performance for the bonded samples. Finally, all sandwich samples were prepared. Fig. 6 shows several examples, and the specifications of the samples are provided in Table 1. Note that to ensure the reliability and repeatability of the results, two identical samples were fabricated

and tested for each unique configuration (see Table 1), resulting in a total of 24 bending tests.

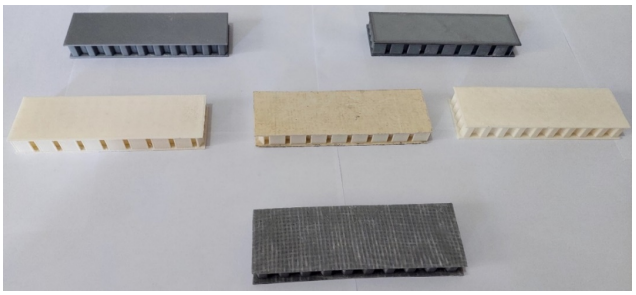

Fig. 6. Sandwich panels with composite facesheets (bottom), separate facesheets (middle), and integrated (top).

Table 1
Sample Specifications. Dimensions of the samples are 18×50×160mm.

Sample description	Sample code	Sample Weight (gr)
Composite ABS Honeycomb	CAH1	63
	CAH2	64
Composite ABS Re-enterant	CAR1	68
	CAR2	69
Composite PLA Honeycomb	CPH1	66
	CPH2	65
Composite PLA Re-enterant	CPR1	69
	CPR2	68
Integrated ABS Honeycomb	IAH1	42
	IAH2	43
Integrated ABS Re-enterant	IAR1	51
	IAR2	53
Integrated PLA Honeycomb	IPH1	49
	IPH2	49
Integrated PLA Re-enterant	IPR1	53
	IPR2	53
Separated ABS Honeycomb	SAH1	49
	SAH2	49
Separated ABS Re-enterant	SAR1	55
	SAR2	56
Separated PLA Honeycomb	SPH1	61
	SPH2	63
Separated PLA Re-enterant	SPR1	64
	SPR2	62

2.2. Mechanical Tests

In this research, three-point bending and tensile tests were performed to evaluate the mechanical properties. Dogbone samples made of PLA and ABS, and rectangular samples of the composite facesheets were tested with a tensile testing machine to accurately determine mechanical properties. A total of 24 fabricated sandwich panel samples underwent three-point bending tests. All bending tests were performed with a 15-ton universal testing machine according to the ASTM C393 standard. Figure 7 shows an image of a sample placed in the bending test machine.

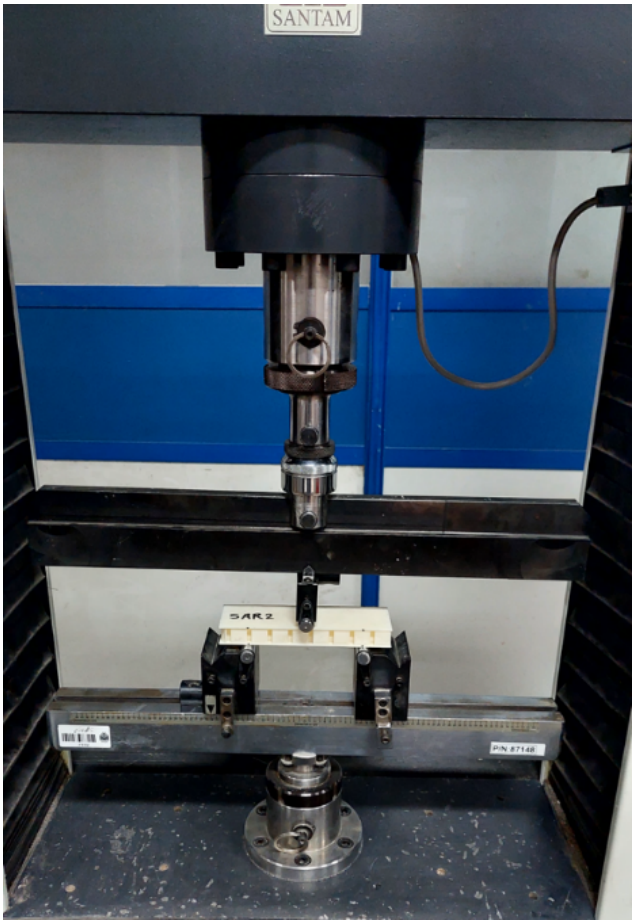

Fig. 7. Sandwich sample in the bending test machine.

The crosshead speed for the bending tests was set to 3mm/min. The tests continued until complete failure occurred. According to the standard, the formulas for core shear stress (τ) and facesheet bending stress (σ) are given by equations (1) and (2), respectively.

$$t = \frac{P}{b(d+c)} \tag{1}$$

$$= \frac{PL}{2t\,(d+c)\,b} \tag{2}$$

In these relations, P is the force, t is the thickness of the sandwich panel, c is the core thickness, b is the width of the sandwich panel, L is the span between supports, and t is the facesheet thickness.

To obtain mechanical properties including elastic modulus and ultimate tensile strength, tensile tests were performed using a SANTAM 5-ton universal testing machine. For composite samples, the ASTM D3039 standard was used. The composite samples of ABS and PLA were prepared as rectangular strips with a width of 20mm and a length of 150mm for testing. The gauge length of the extensometer used for the tensile test was 50mm, and the loading rate for composite samples was 2mm/min. Dogbone-shaped samples were also prepared from PLA and ABS according to ASTM D638. The model of the samples was designed

in SolidWorks software according to the dimensions in the standard and fabricated by the 3D printer. The loading rate for dogbone samples was 5mm/min. Fig. 8 shows these samples.

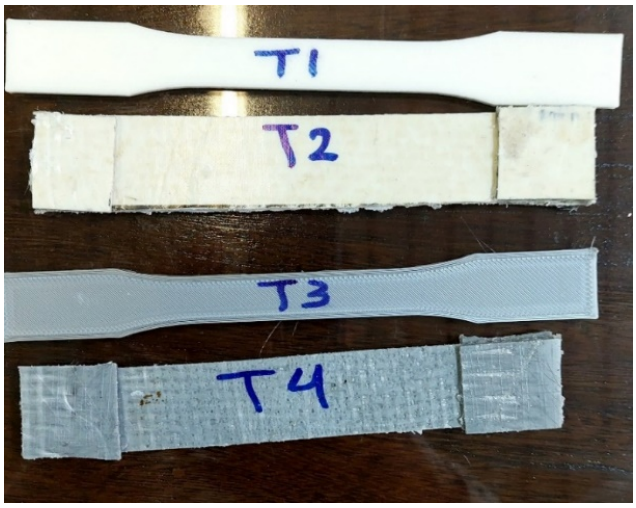

Fig. 8. Samples for tensile test.

3. Results and Discussion

This section presents a detailed analysis of the experimental results, focusing on the tensile properties of the constituent materials, the flexural performance of the various sandwich configurations, their energy absorption characteristics, and the observed failure mechanisms. The findings are interpreted to elucidate the structure-property relationships governing the behavior of the fabricated sandwich panels.

Tensile tests were conducted according to ASTM D638 for polymer samples and ASTM D3039 for composite samples. The tensile test results are shown in Fig. 9.

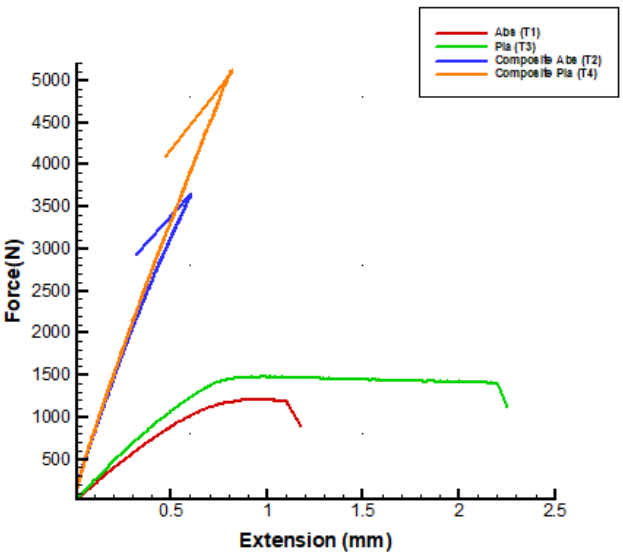

(a)

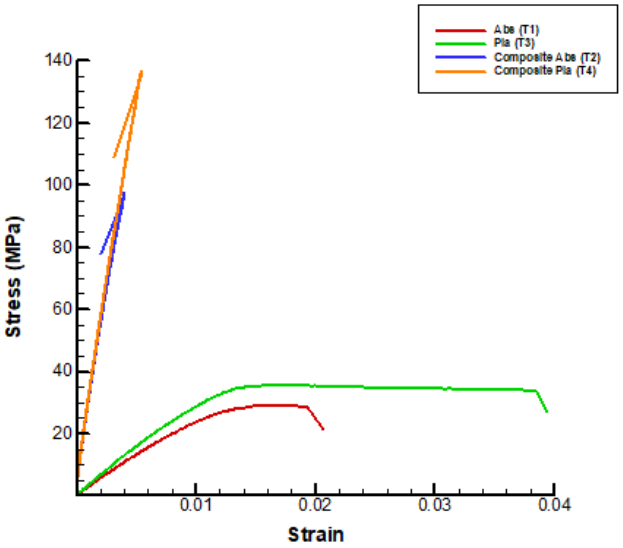

(b)

Fig. 9. Tensile tests of faces; a) force-displacement diagram and b) Stress-strain cures.

The tensile properties of the pure thermoplastic (PLA, ABS) and their respective glass fiber-reinforced composites were characterized, as these directly influence the flexural performance of the sandwich panels. The results, summarized in Table 2, reveal a significant enhancement in mechanical properties due to fiber reinforcement.

Table 2
Elastic modulus, yield strength, and ultimate strength for tensile samples.

Sample	Elastic modulus (MPa)	Yield strength (MPa)	Ultimate strength (MPa)
ABS (T1)	2406.2	22.72	29.09
PLA (T3)	2831.7	29.09	35.55
Composite ABS (T2)	23827	-	97.12
Composite PLA (T4)	24713	-	136.65

The elastic moduli of the composite PLA and composite ABS facesheets were 24.71GPa and 23.82GPa, respectively. This represents an order-of-magnitude increase compared to their neat polymer counterparts (PLA: 2.83GPa, ABS: 2.40GPa). This dramatic improvement in stiffness is a direct consequence of the load-bearing capacity of the continuous glass fibers, which effectively carry the applied stress. Similarly, the ultimate tensile strength of the composites (136.65MPa for PLA-based, 97.12MPa for ABS-based) far exceeded that of the pure polymers (35.55MPa and 29.09MPa, respectively). The higher strength and modulus of the composite PLA compared to composite ABS suggest a potentially stronger interface or better impregnation

between the glass fibers and the PLA matrix during the hot-pressing process. These superior tensile properties of the composite facesheets are anticipated to contribute significantly to the flexural strength and stiffness of the corresponding sandwich panels.

3.1. Flexural Behavior of Sandwich Panels

The fabricated samples were tested according to ASTM C393 standard with a loading speed of 3mm/min. Fig. 10 shows a sample during the three-point bending test.

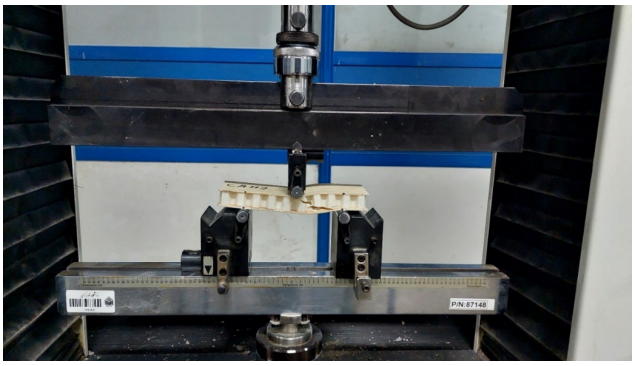

Fig. 10. Sample during bending test.

The results of the three-point bending test for separate samples with composite facesheets made of ABS and PLA with glass fiber and cores with honeycomb and re-entrant geometries are shown in Fig. 11.

The results of the three-point bending test for separate samples made of ABS with honeycomb and re-entrant cores are shown in Fig. 12.

The results of the three-point bending test for integrated samples made of PLA and ABS with honeycomb and re-entrant cores are shown in Fig. 13.

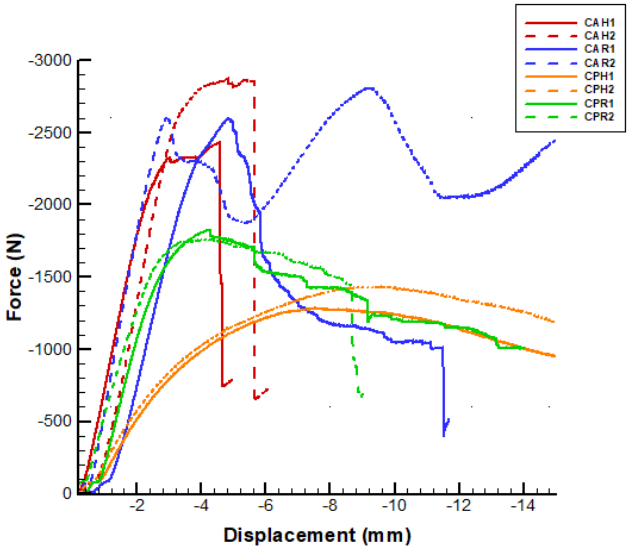

Fig. 11. Force-Displacement diagram of separate samples with composite facesheets.

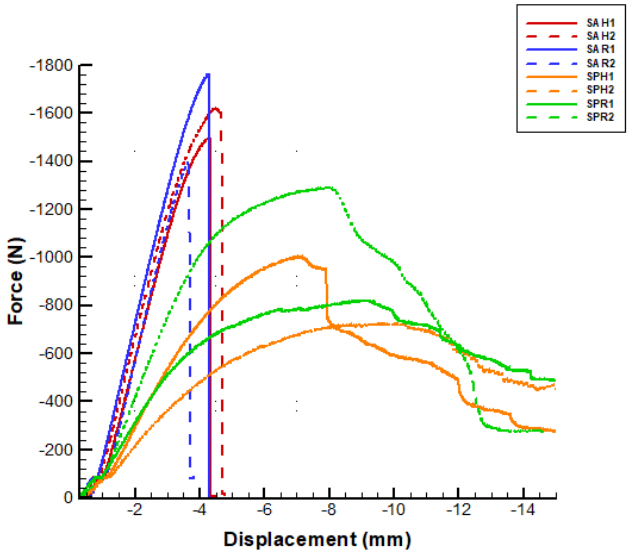

Fig. 12. Force-Displacement diagram of separate samples.

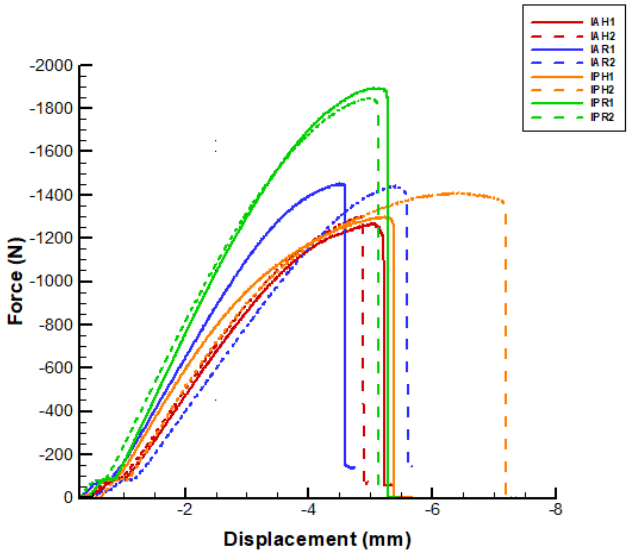

Fig. 13. Force-Displacement diagram of integrated samples.

As evident from Figs. 11 to 13, the samples with re-entrant cores sustained approximately 20% higher loads than their honeycomb-core counterparts. Furthermore, samples with composite facesheets exhibited the highest flexural strength. A critical observation is the superior performance of panels with composite facesheets across all metrics. For instance, samples like CAR2 (Composite ABS, Re-entrant core) sustained peak loads exceeding 2900 N, significantly higher than any integrated or separate sample with pure thermoplastic facesheets, which typically failed below 2000N. This underscores the primary role of high-performance facesheets in carrying bending moments.

The influence of core geometry is also pronounced. In both integrated and composite-faced configurations, panels with re-entrant cores (e.g., CAR, CPR, IAR,

IPR) consistently exhibited higher peak loads and initial stiffness compared to their honeycomb-core counterparts (CAH, CPH, IAH, IPH). This enhancement is attributed to the unique deformation mechanism of the re-entrant architecture. Under bending, the core experiences shear forces. The re-entrant cells, characterized by their negative Poisson's ratio, tend to contract laterally when compressed, leading to a densification of the core material at the load application point. This localized densification enhances shear resistance and delays the onset of core shear failure, thereby allowing the panel to sustain higher loads.

The manufacturing method also played a crucial role. Integrated panels (e.g., IAH, IPR) exhibited stable deformation but generally failed at lower loads than the separate configurations with composite facesheets. This is attributed to the inherent limitations of the fused deposition modeling (FDM) process, where inter-layer adhesion and printing defects can create points of failure. The separate panels with bonded composite facesheets benefited from the superior, monolithic nature of the hot-pressed facesheets and a strong adhesive bond, which effectively transferred stresses between the core and the skins.

The facesheet material demonstrated a profound influence on the structural performance. Composite-faced samples exhibited significantly higher stiffness and load-bearing capacity compared to their thermoplastic counterparts. For instance, CAR samples showed a 92% increase in maximum load compared to IAR samples, underscoring the critical role of high-stiffness facesheets in carrying bending moments. This enhancement is directly attributable to the superior tensile properties of the glass fiber composites, as quantified in Table 2.

Core geometry substantially influenced the failure progression and energy absorption mechanisms. Re-entrant cores consistently delayed catastrophic failure through their unique deformation mechanism. Under bending, the negative Poisson's ratio effect caused the re-entrant cells to contract laterally on the compression side, leading to progressive core densification rather than abrupt shear failure. This resulted in more stable load-displacement curves and higher energy absorption compared to honeycomb cores, which typically failed through sudden cell wall buckling.

The manufacturing method significantly affected structural integrity. Integrated samples, while showing consistent performance (evidenced by low standard deviations in Table 4), were limited by inter-layer adhesion weaknesses inherent to FDM printing. In contrast, the separate configurations with composite facesheets leveraged the monolithic nature of hot-pressed composites, achieving superior performance. The adhesive bond in separate samples effectively transferred stresses, with failure initiating in the core rather than the bond line, confirming the robustness of the bonding technique.

3.2. Energy Absorption of Sandwich Panels

The absorbed energy (Ea) was calculated as the area under the force-displacement curve using Eq. (3). Specific energy absorption (SEA) was also obtained using Eq. (4).

$$Ea = \int_0^{dmax} F(d)dd \tag{3}$$

$$SEA = \frac{Ea}{m} \tag{4}$$

In the above equations, δ_{max} is the maximum displacement and m is the weight of the sandwich sample. Fig. 14 compares the energy absorption capacity of each sample up to the moment of failure.

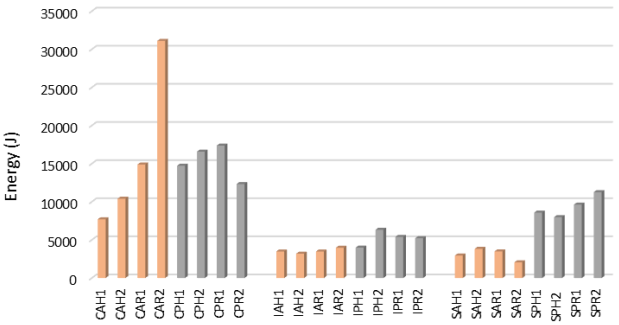

Fig. 14. Comparison of energy absorption of samples until failure.

Table 3 shows the values of energy absorption capacity and specific absorbed energy for the samples.

The results indicate that the composite-faced samples exhibited the highest energy absorption (up to 20kJ). The integrated structures exhibited more stable behavior under loading due to their monolithic construction.

Fig. 15 shows the maximum force that the samples could bear. The composite samples bore the highest load for both integrated and separate configurations. Samples with re-entrant cores also withstood higher forces than those with honeycomb cores. Furthermore, for composite and separate samples, ABS samples withstood more force than PLA samples. However, in integrated samples, PLA withstood more force than ABS.

Fig. 16 shows the maximum displacement of the samples before failure. Composite-faced samples exhibited the greatest deflection, followed by separate and then integrated samples.

Table 4 provides the values of maximum force, bending stress in the facesheets, core shear stress, and maximum deflection for the samples. The quantitative results presented in Table 4 demonstrate good repeatability for most configurations, as indicated by the relatively low standard deviations compared to the mean values. For instance, integrated samples

and composite-faced re-entrant samples showed particularly consistent performance. Higher variability was observed in some separate thermoplastic samples (e.g., SPR, SAR), which can be attributed to slight inconsistencies in the adhesive bonding process or inherent print defects, highlighting the challenge of manual fabrication compared to the more automated and monolithic integrated and hot-pressed methods.

Table 3
Energy absorption capacity and specific energy absorption of samples.

CAH1	7.70	122.22
CAH2	10.40	162.50
CAR1	14.89	218.97
CAR2	31.11	450.87
CPH1	14.73	223.18
CPH2	16.57	254.92
CPR1	17.37	251.74
CPR2	12.33	181.32
IAH1	3.48	82.86
IAH2	3.19	74.19
IAR1	3.47	68.04
IAR2	3.97	74.91
IPH1	3.99	81.43
IPH2	6.33	129.18
IPR1	5.39	101.70
IPR2	5.22	98.49
SAH1	2.95	60.20
SAH2	3.83	78.16
SAR1	3.49	63.45
SAR2	2.05	36.61
SPH1	8.58	140.66
SPH2	7.98	126.67
SPR1	9.63	150.47
SPR2	11.27	181.77

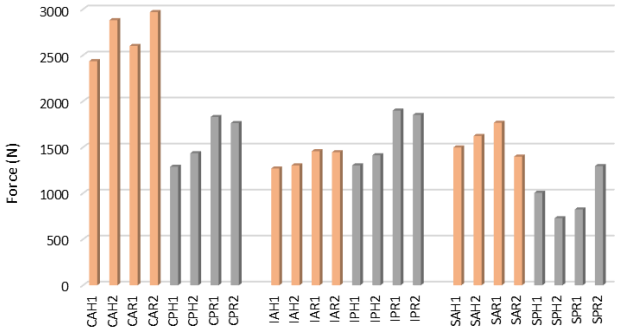

Fig. 15. Chart of maximum bearable force of samples.

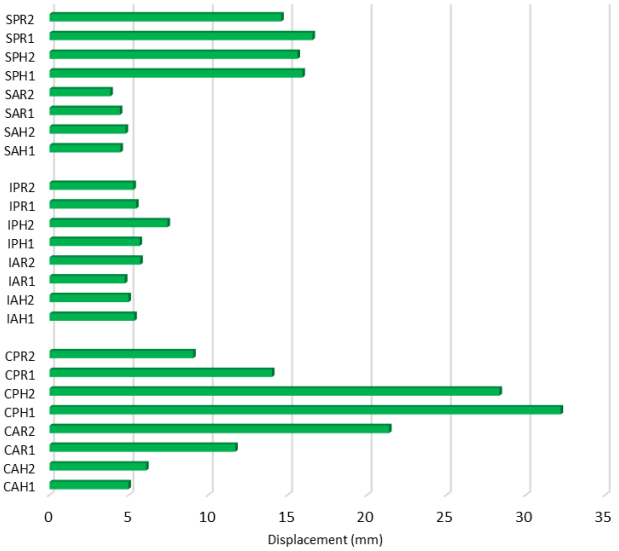

Fig. 16. Comparison of maximum displacement of samples until failure.

Table 4
Mean values and standard deviations for maximum force (P), bending stress in facesheets (σ), core shear stress (τ), and maximum deflection.

Sample Type	P (N)	σ (MPa)	τ (MPa)	δ (mm)
Composite ABS Honeycomb (CAH)	2657.9 ± 315.1	59.06 ± 6.99	1.61 ± 0.19	5.53 ± 0.79
Composite ABS Re-entrant (CAR)	2784.9 ± 260.3	61.89 ± 5.78	1.69 ± 0.16	16.54 ± 6.85
Composite PLA Honeycomb (CPH)	1361.2 ± 104.0	30.25 ± 2.31	0.83 ± 0.06	30.27 ± 2.73
Composite PLA Re-entrant (CPR)	1795.2 ± 46.6	39.89 ± 1.04	1.09 ± 0.03	11.53 ± 3.51
Integrated ABS Honeycomb (IAH)	1285.8 ± 23.4	28.57 ± 0.52	0.78 ± 0.01	5.16 ± 0.26
Integrated ABS Re-entrant (IAR)	1451.3 ± 7.8	32.25 ± 0.17	0.88 ± 0.00	5.23 ± 0.68
Integrated PLA Honeycomb (IPH)	1357.5 ± 77.9	30.17 ± 1.73	0.82 ± 0.05	6.55 ± 1.24
Integrated PLA Re-entrant (IPR)	1874.3 ± 33.8	41.65 ± 0.75	1.14 ± 0.02	5.37 ± 0.12
Separated ABS Honeycomb (SAH)	1559.8 ± 88.4	34.66 ± 1.96	0.95 ± 0.05	4.63 ± 0.23
Separated ABS Re-entrant (SAR)	1581.9 ± 260.1	35.15 ± 5.78	0.96 ± 0.16	4.13 ± 0.42
Separated PLA Honeycomb (SPH)	866.4 ± 195.1	19.25 ± 4.34	0.53 ± 0.12	15.78 ± 0.22
Separated PLA Re-entrant (SPR)	1059.5 ± 332.8	23.54 ± 7.39	0.64 ± 0.20	15.58 ± 1.39

The force-displacement diagrams for all composite, separate, and integrated configurations are presented in Fig. 17.

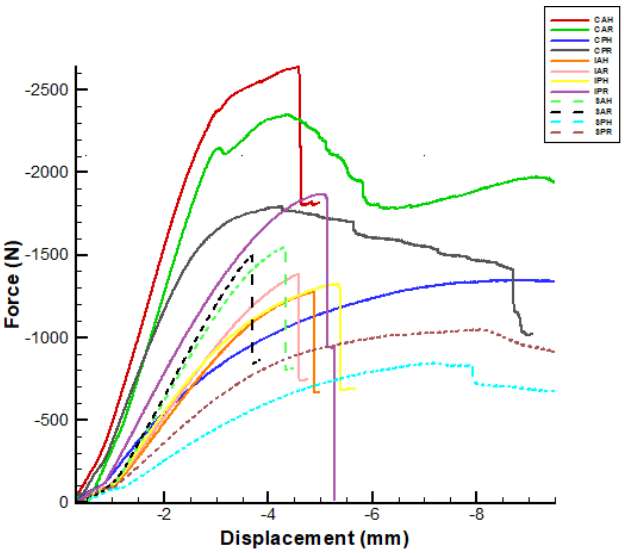

Fig. 17. Comparison of Force-Displacement diagrams for all samples.

Fig. 18 compares the maximumforce values for all sample types.

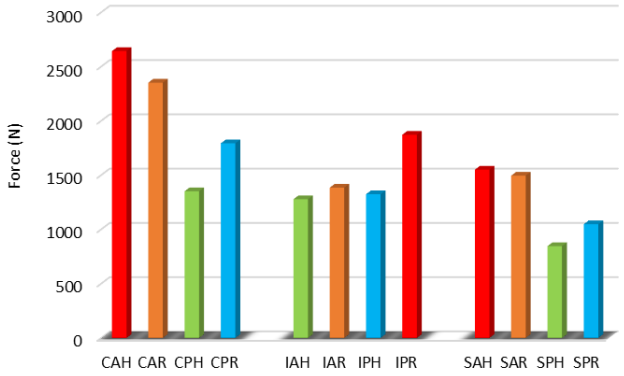

Fig. 18. Bearable force values of samples.

Fig. 19 compares the energy absorbed by each sample.

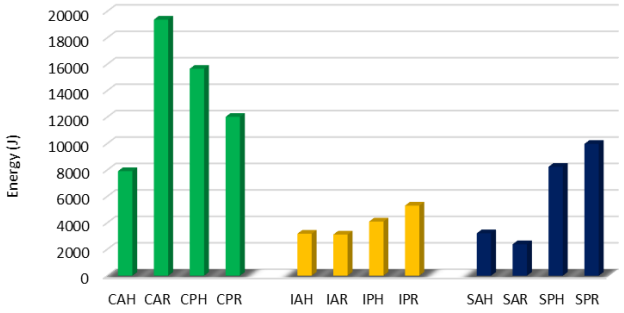

Fig. 19. Comparison of energy absorption values of samples.

It should be noted that Figs. 17, 18, and 19 are plotted using the average values of two samples per type to provide a better understanding of the behavior of each structure type.

The energy absorption capacity, calculated as the area under the load-displacement curve, and the specific energy absorption (*SEA*) are critical parameters for applications involving impact or crashworthiness. The results, graphically compared in Fig. 19 and quantified in Table 3, demonstrate a clear hierarchy.

Panels with composite facesheets and re-entrant cores displayed the most outstanding energy absorption performance. For example, sample CAR2 achieved an absorbed energy (*Ea*) of 31.11kJ and a remarkable *SEA* value of 450.87kJ/kg. This is substantially higher than the best-performing integrated sample (IPH2 with Eα of 6.33kJ and *SEA* of 129.18kJ/kg) or separate thermoplastic sample (SPR2 with *Ea* of 11.27kJ and *SEA* of 181.77kJ/kg). The high energy absorption in composite-faced panels is a direct result of the combination of high load-bearing capacity (high force) and significant ductility (large displacement before failure), as seen in their extended load-displacement curves (Fig. 11).

The re-entrant core geometry again proved advantageous over the honeycomb for energy absorption. The progressive collapse and densification of the re-entrant cells, as opposed to a more brittle failure often observed in honeycombs, allows for a larger area under the curve. This makes the re-entrant core particularly effective for dissipating mechanical energy.

For better analysis of the structures, Table 5 provides the values of key flexural parameters (maximum load, flexural modulus, SEA, and failure strain) for all sample configurations.

The specific energy absorption (SEA) values in Tables 3 and 5 provide a clear performance hierarchy. Composite-faced re-entrant cores (CAR) achieved the highest SEA (334.9±164.2kJ/kg), demonstrating the synergistic effect of high-strength facesheets and an energy-absorbing core geometry. The substantial standard deviation for CAR samples reflects the sensitive nature of the re-entrant structure's collapse mechanism, which can be optimized for more consistent performance in future iterations. The data in Table 3 further reveal that samples with PLA matrices generally show higher energy absorption capacity compared to their ABS counterparts, which can be attributed to PLA's higher fracture toughness.

The standard deviations presented in Tables 4 and 5 provide valuable insights into the manufacturing consistency. Integrated samples exhibited the lowest variability, confirming the reproducibility of 3D printing for these structures. The higher variability observed in some composite and separated samples, particularly those with re-entrant cores, highlights the sensitivity of these advanced configurations to manufacturing parameters and suggests areas for process optimization in future work.

Table 5
Mean values and standard deviations of key flexural parameters for all sample configurations.

Sample type	Max load (N)	Flexural modulus (MPa)	Specific energy absorption (kJ/kg)	Failure strain (%)
Composite ABS Honeycomb (CAH)	2657.9 ± 315.1	1245.3 ± 85.2	142.4 ± 28.5	4.2 ± 0.6
Composite ABS Re-entrant (CAR)	2784.9 ± 260.3	1389.7 ± 92.1	334.9 ± 164.2	8.5 ± 2.1
Composite PLA Honeycomb (CPH)	1361.2 ± 104.0	987.6 ± 45.3	239.1 ± 22.5	12.8 ± 1.5
Composite PLA Re-entrant (CPR)	1795.2 ± 46.6	1156.8 ± 38.9	216.5 ± 49.8	6.8 ± 1.2
Integrated ABS Honeycomb (IAH)	1285.8 ± 23.4	845.2 ± 15.8	78.5 ± 6.1	3.5 ± 0.3
Integrated ABS Re-entrant (IAR)	1451.3 ± 7.8	923.6 ± 12.4	71.5 ± 4.9	3.2 ± 0.4
Integrated PLA Honeycomb (IPH)	1357.5 ± 77.9	891.3 ± 28.7	105.3 ± 33.8	4.1 ± 0.8
Integrated PLA Re-entrant (IPR)	1874.3 ± 33.8	1102.4 ± 25.6	100.1 ± 2.3	3.1 ± 0.2
Separated ABS Honeycomb (SAH)	1559.8 ± 88.4	765.4 ± 32.1	69.2 ± 12.7	3.2 ± 0.2
Separated ABS Re-entrant (SAR)	1581.9 ± 260.1	812.5 ± 45.8	50.0 ± 19.0	2.8 ± 0.3
Separated PLA Honeycomb (SPH)	866.4 ± 195.1	523.7 ± 67.4	133.7 ± 9.9	9.8 ± 0.1
Separated PLA Re-entrant (SPR)	1059.5 ± 332.8	587.2 ± 89.3	166.1 ± 22.1	9.2 ± 0.8

3.3. Failure Modes of Sandwich Panels

Failure modes that may occur for a sandwich panel include core failure, facesheet failure, facesheet wrinkling, and debonding between the facesheet and core. The failure modes observed in the three-point bending test for the samples are presented below.

In composite samples, the primary failure mode was core failure followed by facesheet debonding, as shown in Fig. 20.

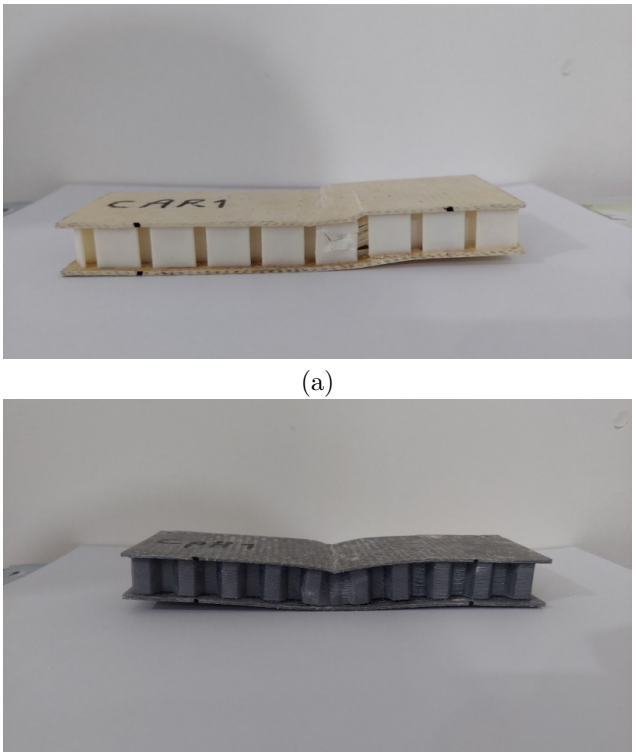

(a)

(b)

Fig. 20. Composite samples after failure; a) Sample CAR1, b) Sample CPH1.

In separate samples, the primary failure mode was core failure followed by facesheet failure. This mode is shown in Fig. 21.

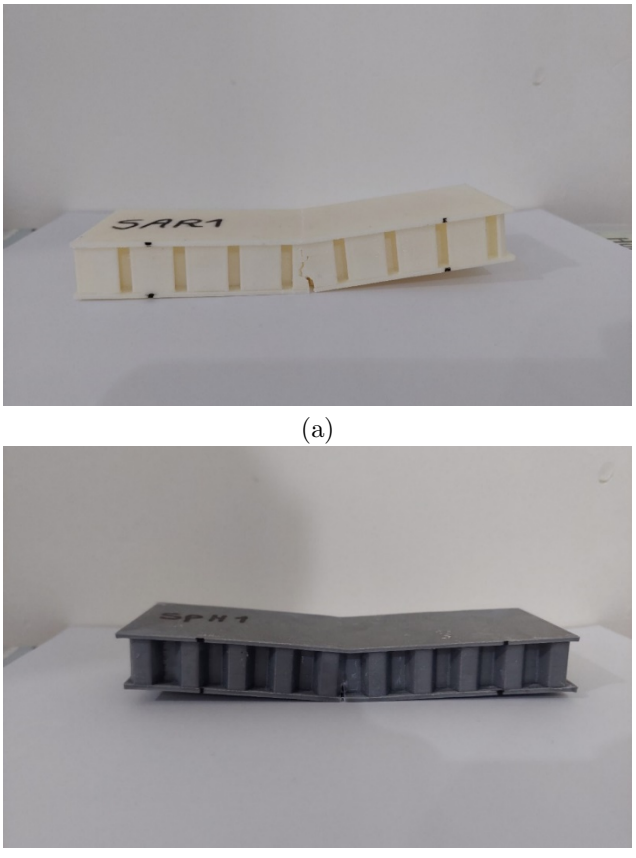

(a)

(b)

Fig. 21. Separate samples after failure; a) Sample SAR1, b) Sample SPH1.

In integrated samples, the primary failure mode was simultaneous failure of the facesheet and core. This mode is shown in Fig. 22.

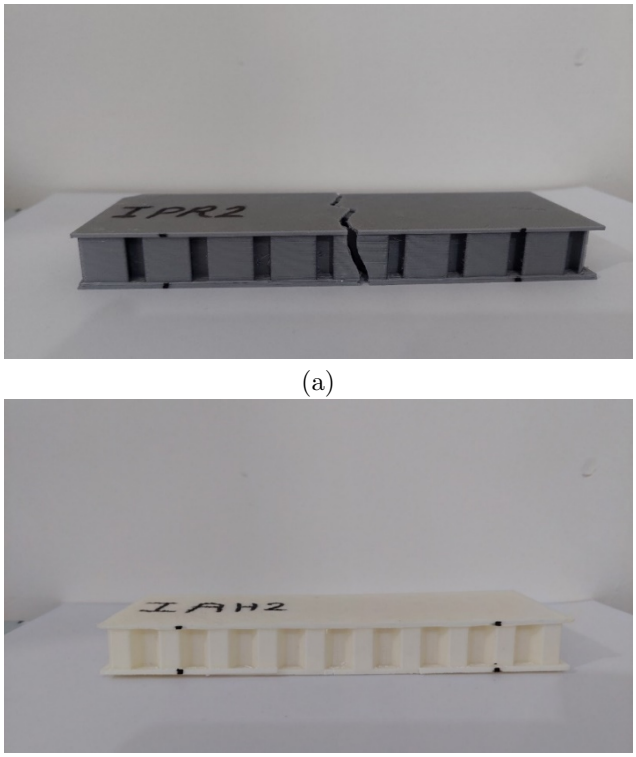

(a)

(b)

Fig. 22. Integrated samples after failure; a) Sample IAH2, b) Sample IPR2.

The failure modes, illustrated in Figs. 20-22, were directly influenced by the panel's construction. The integrated panels (Fig. 22) predominantly failed through simultaneous cracking of the core and the printed facesheets. This is characteristic of monolithic FDM structures where stress concentrations at the layer interfaces lead to catastrophic failure.

The separate panels with thermoplastic facesheets (Fig. 21) typically exhibited a sequential failure: initial core shear failure, followed by the failure of the adhesively bonded facesheets. This indicates that the core was the weakest link in these configurations.

The most complex yet desirable failure mode was observed in the composite-faced panels (Fig. 20). The primary failure initiated as shear cracking within the core. However, the robust composite facesheets did not fracture catastrophically but instead underwent progressive debonding (delamination) from the core. This ductile failure mode, involving core crushing and facesheet debonding, allows for continued load carriage and large energy dissipation even after the initial failure, explaining their superior performance in terms of both maximum displacement and total energy absorbed.

The distinct failure patterns observed across different configurations directly result from their structural architecture and material properties. In integrated samples, the simultaneous facesheet and core failure occurs due to stress concentrations at the printed layer interfaces, which act as pre-existing flaw sites. The monolithic nature of FDM structures causes crack propagation through the weakest inter-layer bonds, leading to catastrophic failure. For separate thermoplastic samples, the sequential failure initiates in the core because the thermoplastic facesheets possess higher ductility than the printed core structures. The core fails first in shear due to its lower shear modulus, followed by facesheet failure once the load redistribution exceeds their capacity. The most desirable failure mode in composite-faced panels results from the stiffness mismatch between the high-modulus facesheets and the relatively compliant core. Failure initiates as shear cracking in the core, but the robust facesheets resist catastrophic fracture. Instead, progressive debonding occurs at the interface, allowing for continued load carriage through friction and mechanical interlocking. This failure sequence maximizes energy absorption by utilizing multiple dissipation mechanisms and preventing sudden collapse.

In conclusion, the synergy between high-stiffness composite facesheets and a shear-resistant, energy-absorbing re-entrant core geometry yields a sandwich panel configuration with exceptional flexural performance and energy absorption capacity, making it a promising candidate for advanced lightweight structural applications.

4. Conclusion

The growing application of sandwich panels across industries underscores the value of developing recyclable and remanufacturable structures, which contribute to environmental preservation, pollution reduction, and lower production costs. In this study, sandwich panels in integrated and separate forms with honeycomb and re-entrant cores made from environmentally compatible materials, PLA and ABS, were fabricated using a 3D printer. Additionally, samples with composite facesheets made from glass fibers and shredded PLA and ABS filaments were produced. The composite facesheets, consisting of two layers of glass fiber, were fabricated using an effective hot press method, contributing to increased strength and resistance to environmental factors. The core dimensions were 15×50×160mm and the facesheet thickness was 1.5mm. A total of 24 samples were subjected to three-point bending tests and 4 samples to tensile tests to obtain the mechanical properties of the sandwich panels. The weight of the structures was approximately 42-70 grams.

Core shear stress, facesheet bending stress, maximum bearable load, absorbed energy, and displacement before failure were calculated and compared for the tested samples. The main findings of this study are summarized as follows:

1) The use of re-entrant cores and composite

facesheets significantly improves the flexural behavior and energy absorption of sandwich panels. Samples with re-entrant cores sustained approximately 20% higher loads than their honeycomb counterparts.

2) The maximum load-bearing capacity of composite-faced samples was superior to that of both integrated and separate samples with thermoplastic facesheets.

3) Composite-faced samples exhibited the highest energy absorption, followed by separate and then integrated samples, demonstrating the benefit of the robust, hot-pressed facesheets and strong adhesive bond.

4) Failure modes were directly linked to the manufacturing method, with integrated panels failing catastrophically, separate thermoplastic panels failing via core shear, and composite-faced panels failing through progressive core crushing and facesheet debonding, which contributed to their high energy absorption.

This study demonstrates that 3D printing and hot pressing are effective methods for producing stable and environmentally compatible structures. The optimal configuration—re-entrant cores with composite facesheets—shows great promise for applications in lightweight transportation, protective packaging, and sustainable construction, where high specific strength and energy absorption are critical.

References

[1] J. Kee Paik, A. K. Thayamballi, G. Sung Kim. Strength characteristics of aluminum honeycomb sandwich panels, Thin-Walled Struct., 35(3) (1999) 205–231.

[2] J. H. Lee, S. H. Kang, Y. J. Ha, S. G. Hong. Structural Behavior of Durable Composite Sandwich Panels with High Performance Expanded Polystyrene Concrete, Int. J. Concr. Struct. Mater., 12(1) (2018) 14.

[3] L. Zhang, Y. Chen, R. He, X. Bai, K. Zhang, S. Ai, Y. Yang, D. Fang. Bending behavior of lightweight C/SiC pyramidal lattice core sandwich panels, Int. J. Mech. Sci., 171 (2020) 105409.

[4] J. Wetzel. The impulse response of extruded corrugated core aluminum sandwich structures, Ph.D. dissertation, University of Virginia, (2009).

[5] J. M. Davies, Sandwich panels. Thin-Walled Struct., 16(1-4) (1993) 179-198.

[6] A. Cherniaev. Modeling of hypervelocity impact on open cell foam core sandwich panels, Int. J. Impact Eng., 155 (2021) 103901.

[7] A. B. H. Kueh and Y. Y. Siaw. Impact resistance of bio-inspired sandwich beam with side-arched and honeycomb dual-core, Compos. Struct., 275 (2021) 114439.

[8] I. Kreja. A literature review on computational models for laminated composite and sandwich panels, Cent. Eur. J. Eng., 1(1) (2011) 59-80.

[9] Y. Hou, Y. H. Tai, C. Lira, F. Scarpa, J. R. Yates, and B. Gu. The bending and failure of sandwich structures with auxetic gradient cellular cores, Compos. Part A Appl. Sci. Manuf., 49 (2013) 119-131.

[10] H. Yazdani Sarvestani, A. H. Akbarzadeh, H. Niknam, and K. Hermenean. 3D printed architected polymeric sandwich panels: Energy absorption and structural performance, Compos. Struct., 201 (2018) 1122-1133.

[11] R. M. Jones. Mechanics of Composite Materials, 2nd ed. Boca Raton, FL, USA: CRC Press, (1998).

[12] R. E. Shalin, Ed. Polymer Matrix Composites. Boston, MA, USA: Springer, (1998).

[13] M. R. Kessler. Polymer Matrix Composites: A Perspective for a Special Issue of Polymer Reviews, Polym. Rev., 52(3-4) (2012) 229-233.

[14] M. Elkington, D. Bloom, C. Ward, A. Chatzimichali, K. Potter. Hand layup: understanding the manual process, Adv. Manuf. Polym. Compos. Sci., 1(3) (2015) 138-151.

[15] R. O. Buckingham, G. C. Newell. Automating the manufacture of composite broadgoods, Compos. Part A Appl. Sci. Manuf., 27(3) (1996) 191-200.

[16] T. Li, L. Wang. Bending behavior of sandwich composite structures with tunable 3D-printed core materials, Compos. Struct., 175 (2017) 46-57.

[17] M. Aadithya, V. K. Kirubakar, T. Aakash, C. Senthamaraikannan. Investigation of the tensile and flexural behavior of polylactic acid based jute fiber bio composite, Key Eng. Mater., 841 (2020) 283-287.

[18] I. Ozen, K. Cava, H. Gedikli, U. Alver, M. Aslan. Low-energy impact response of composite sandwich panels with thermoplastic honeycomb and reentrant cores, Compos. Struct., 252 (2020) 112699.

[19] X. Hao, H. Zhou, Y. Xie, H. Mu, Q. Wang. Sandwich-structured wood flour/HDPE composite panels: Reinforcement using a linear low-density polyethylene core layer, Constr. Build. Mater., 164 (2018) 489-496.

[20] F. Habib, F. N. Habib, P. Iovenitti, S. H. Masood, M. Nikzad. Fabrication of polymeric lattice structures for optimum energy absorption using Multi Jet Fusion technology, Mater. Des., 155 (2018) 86-98.

[21] H. Xie, C. Shen, H. Fang, J. Han, W. Cai. Flexural property evaluation of web reinforced GFRP-PET foam sandwich panel: Experimental study and numerical simulation, Compos. Part B Eng., 234 (2022) 109725.